Engineering Science and Technology, an International Journal 18 (2015) 351–360

HOSTED BY

Contents lists available at ScienceDirect

Engineering Science and Technology, an International Journal

journal homepage: http://www.elsevier.com/locate/jestch

Full length article

Modeling and performance optimization of automated antenna alignment for telecommunication transceivers

Md. Ahsanul Hoque [a, *], Ahmad Kamal Hassan [b, c]

[a] Department of Electrical & Electronic Engineering, Int'l Islamic University Chittagong (IIUC), Kumira, Chittagong 4314, Bangladesh
[b] Department of Electrical and Computer Engineering, Faculty of Engineering, King Abdulaziz University, P.O. Box 80204, Jeddah 21589, Saudi Arabia
[c] Center of Excellence in Intelligent Engineering Systems (CEIES), King Abdulaziz University, Jeddah, Saudi Arabia

ARTICLE INFO

Article history:
Received 4 November 2014
Received in revised form
26 December 2014
Accepted 15 January 2015
Available online 16 February 2015

Keywords:
Robotics
Communication
RCX Robonics
Microwave

ABSTRACT

Antenna alignment is very cumbersome in telecommunication industry and it especially affects the MW links due to environmental anomalies or physical degradation over a period of time. While in recent years a more conventional approach of redundancy has been employed but to ensure the LOS link stability, novel automation techniques are needed. The basic principle is to capture the desired Received Signal Level (RSL) by means of an outdoor unit installed on tower top and analyzing the RSL in indoor unit by means of a GUI interface. We have proposed a new smart antenna system where automation is initiated when the transceivers receive low signal strength and report the finding to processing comparator unit. Series architecture is used that include loop antenna, RCX Robonics, LabVIEW interface coupled with a tunable external controller. Denavit–Hartenberg parameters are used in analytical modeling and numerous control techniques have been investigated to overcome imminent overshoot problems for the transport link. With this novel approach, a solution has been put forward for the communication industry where any antenna could achieve optimal directivity for desired RSL with low overshoot and fast steady state response.

1. Introduction

In Telecommunication industry; there are number of equipments installed ranging from Base Transceiver Station (BTS) to Core and Back Haul Network. The most vital aspect that is desired in network connectivity is served by transmission links and its reliability is of utmost importance. It not only enables the connectivity of terminal and linking stations with the core network but also ensures traffic management functionality. Transmission nodes being employed today mostly utilize wired fiber optic links as well as wireless links in MW range. Short and long haul links and Fiber To The Home (FTTH) are wired fiber optic links and consequently various vendors such as Ericsson and Nokia Siemens Networks (NSN) have designed equipment that include HiT, OMS and Flexi-XC. In this paper the prime focus is on the wireless links which can accommodate both STM as well as E1/T1 level data rate. Over here we are particularly interested in the Abis and A interface that are specifically working in MW range. In general practice two different stations are wirelessly linked by means of antenna on either end with proper Line of Sight (LOS). Multiple antennas can be utilized for redundancy with extension of Warm and Hot spares stand-by. The Quality of Service (QoS) pertaining to transmission link is measured by means of Received Signal Level (RSL) measured through either Multi-Meter or by means of a software provided by the antenna manufacturer [1,2]. Fig. 1.1 shows link parameters for a 1 + 0 antenna operating at 38 GHz with low end frequency of 38.1115 GHz and high end frequency of 39.3715 GHz. Antenna directivity originally set can be affected by natural wear out of physical mounts or by environmental anomalies thus misdirecting the main lobe direction of antenna. A manual alignment is carried out that requires high altitude rigger work which is time consuming and risky. Mean Down Time (MDT) caused by such events and procedures results in high economic loss and service unavailability for the customers over extended periods [1,3].

Fig. 1.1, indoor unit is denoted by "MMU" magazine which is tunable to desired frequency and power ratings. This unit is interfaced with an out-door unit "RAU" which is a radio operating at 38 GHz. This specific depiction is of an MW link which is broken

* Corresponding author.
E-mail addresses: ahsan_03@yahoo.com, ahsan.eee03@gmail.com (Md.A. Hoque).
Peer review under responsibility of Karabuk University.

http://dx.doi.org/10.1016/j.jestch.2015.01.002

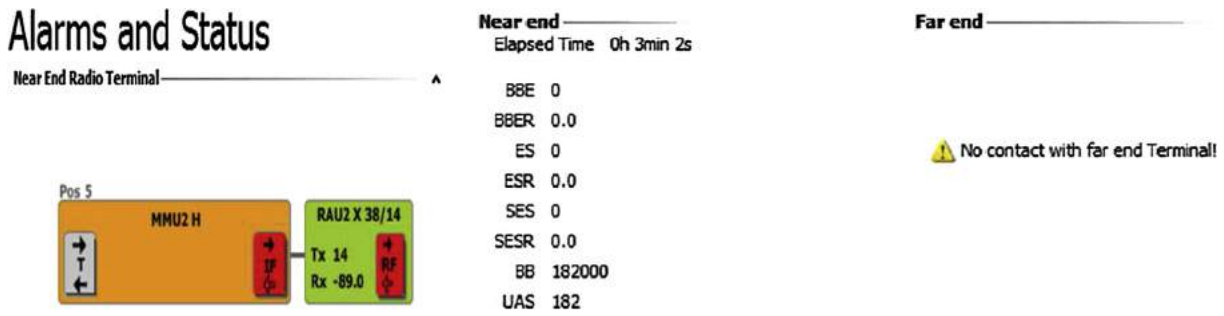

Fig. 1.1. Link parameters to be adjusted for communication.

and needs to be established by means of alignment. The other parameters mentioned are Background Clock (BB) which discards the undesired RF signals by considering them as noise, Background Block Errors (BBE) indicates the errors while filtering process and it is quite evident that present link is not affected because of interference. Certain other parameter's such as Error Seconds (ES), Sensitive Error Seconds (SES) and Unavailable Seconds (UAS) are defining the status of an RF link along with their respective ratios. UAS is indicating a complete link failure and it is the prime factor of assigning critically of any link in industrial environment.

All the aforementioned parameters must be in optimal level to establish a radio link. Because of misalignment far end terminal shows No contact as like in Fig. 1.1. Among of several reasons of link failure, low RSL is one of the most frequent causes, in the given link, RSL level is −89.0 dBm and needs an alignment for link and service restoration. In multiple surveys conducted [4], it can be deduced that the link alignment is not one off job and there is a high possibility for antenna to lose its optimal directivity and hence misdirect the main beam. There could be multiple reasons behind the misalignment such as environmental conditions, wear and tear of mounts and obstruction in the path of two stations. Previously, in 2013 a servo controlled antenna orientation for Satellite Ground Station was presented [5] while a Near Field UHF RFID for multi-antenna systems was proposed in [6] in June 2013. Use of DC motors and hydraulic actuators for the purpose of antenna driving by means of Linear Quadratic Gaussian (LQG) and some fundamental insight about antenna alignment for space application are explored in Ref. [7]. Our work is primarily focused on telecommunication aspects of antenna alignment aimed at reducing the outage and down time to its absolute minimum. This paper deals with analytical and numerical modeling of the antenna alignment prototype for performance optimization, a section of it has been included to investigate the interference from other nodes [8,9]. In 2011, a fundamental approach was presented in Ref. [10] at ATNAC with some basic design analysis and exploration of the domain while here a detailed approach, numerical methods utilized and implementation is presented. Overview of the prototype presented in ATNAC conference; processor was LEGO Mindstorms RCX coupled with control input from LabVIEW design [11] utilization and loop antenna for intended RSL measurement. Here, RCX controller technique used for prototype antenna alignment have built-in PID controller. Realignment of antenna is measured with some derivative gain, steady state response, etc. and hence it directs to optimize the performance through mathematical modeling and by minimizing unexpected overshoot. Different automation techniques for numerous applications have been employed with the main focus on reestablish communication link with minimum down time. Gawronski [15] has worked with pointing and control challenges for large antennas and telescopes. There antenna control system consists of the rate and position feedback loops whose mechanism is developed using controllers like PI controller, LQG, etc. Nourin Kadir et al. in 2011 [16] has worked regarding the tracking system improvement for satellite laser communication, where they have used PID controller to improve system performance on tracking

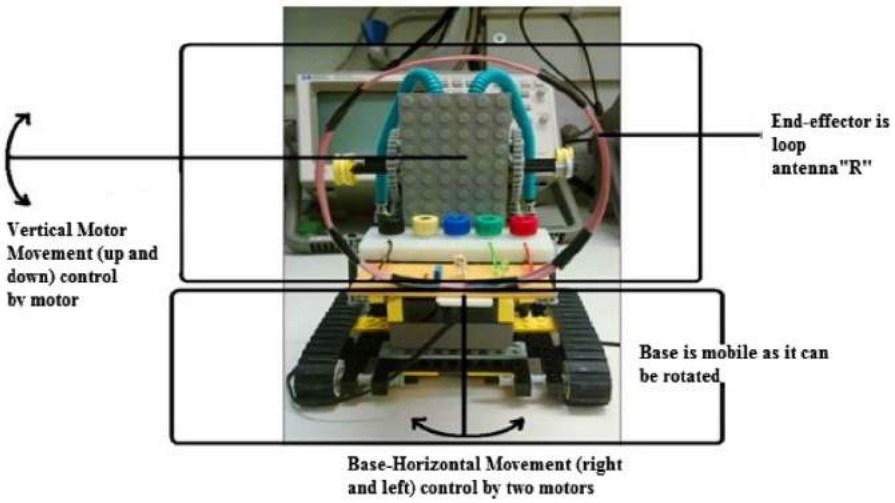

Fig. 2.1. Analyzing the side-wise and lateral movement of model solution.

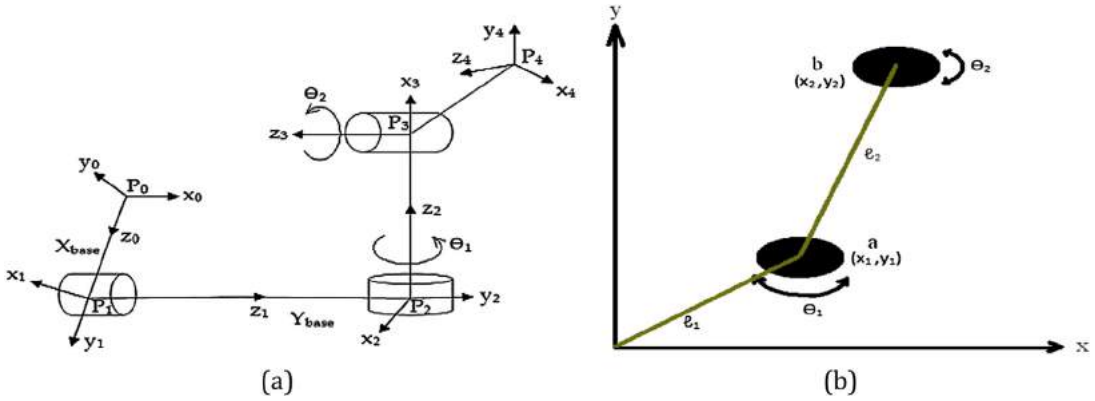

Fig. 2.2. (a) D–H frames for automation system. (b) Two DOF representation on *x* and *y* axes.

compare to feed forward controller. Rafael and Gonçalves in 2012 [17] implemented fuzzy controller to control the alignment mechanism for maneuvering parabolic dish antenna used in satellite communication. In Ref. [18] a work on similar scope using fuzzy logic has been done. Instead of observing the antenna type or system, one common factor similar in all the research papers is control mechanism and controller efficiency by which we can solve alignment issue of antennas within shortest time.

Organization of this report is such that after introduction, mathematical modeling of the automation system by using D–H parameters is discussed in Section 2. Section 3 deals with an overview of the model represented using PID and an analytical modeling to establish transfer function. Section 4 presents the system response time and methods to decrease the overshoot problems encountered during implementation phase. Lastly, the report is concluded in Section 5 which is followed by Acknowledgement and References.

2. Mathematical modeling

In the modeled solution, we have a mobile platform capable of moving in rotational axis for horizontal tilting of end-effecter; which in our case is the Receiver Loop Antenna "R". The means of rotational movement is a double sided conveyor located on either side of the modeled solution. By appropriately programming the controller, both back and forth movement as well as rotational movement can be achieved here we are only concerned with the later problem. Second desired task of automation here is vertical tilting and for that another motor is used. End-effecter "R" is connected with a "Revolt Joint" which actuates the lateral movement. The divisional analysis for the structure is shown in Fig. 2.1.

In the modeled solution, the Degree of Freedom (DOF) referring to the number of joints or rotational axis is 2 and as shown in the above depiction the numbers of actuators are 3 which is shown in detail in Fig. 2.2(a) and (b). For horizontal tilting, two motors are used and thus it makes the horizontal motion controllable and redundant. For vertical tilting, a single motor is used and all motions of the overall system are controllable. All these actuating units are used to position the end-effector (receiver) to achieve the desired RSL. To better understand the position of end-effecter, we can resort to Fig. 2.2(a). Consider θ_1 and θ_2 to be the angle of tilt in horizontal and vertical axis respectively while ℓ_1 and ℓ_2 are the lengths of horizontal and vertical actuators placed on positions "a" and "b" as shown in Fig. 2.2(b). The system is represented in 2-D approach of *x* and *y* axes and is a forward kinematics automation.

In order to understand the position and target point of "R", Denavit–Hartenberg parameters are investigated [12]. The model shown in Fig. 2.2(a) is synthesized into D–H frames to analyze the mechanics involved for overall automation. In the present system, we have a mobile base and a manipulator consisting of 1 joint for vertical tilting. The number of links can be found by adding a unitary value to the total number of joints and this makes our model solution to be a "2 Link Manipulator on a Mobile Base". The manipulator design with reference to D–H frames is shown in Fig. 2.2(b). Reference frame "P_r" is used to take into account the "mobile" base. From Refs. [12–14] a generic homogenous transformation can be formulated using D–H parameters presented in Table 2.1. Since the off-set distance is variable due to the mobile base of unit, it is represented by X_{base} and Y_{base} respectively. The length of the link "*l*" for end-effector is considered of unit length to address the position in simplified manner.

Parameters θ_i and α_i are the joint angle and link twist angle while a_i and d_i are the link length and link offset distance respectively. θ_i is usually the only variable but with the specific case of mobile base, d_i values also change. α_i and a_i are always constants. Referred to Table 2.1, joint angle θ_i will be $\pi/2$ for links 1 and 2 because, both link rotate without axis-transition. Moreover, base joint angle in our prototype have a maximum rotation of $\pi/2$ for its conveyor belt. On the other hand, link 3 and link 4 indicate vertical rotation intended to achieve maximum RSL. Angles θ_1 and θ_2 are dependent variables used to optimize end effecter. Joint twist angle α_i has a predefined value for links 1, 2 and 3, this is because horizontal and vertical motion of motor should attain maximum RSL from 0° to ±45° i.e. 90° or $\pi/2$ of maximum rotation. At the same time, link 4 should not rotate the end effector at maximum RSL, so it will remain at 0° angle. Using homogenous transformation matrices, the position and orientation of end-effecter with respect to the reference "P_r" can be generalized as

$$A = \mathrm{Rot}_{z,\theta_i}\mathrm{Trans}_{z,d_i}\mathrm{Trans}_{x,a_i}\mathrm{Rot}_{x,a_i} \tag{2.1}$$

where, $\mathrm{Rot}_{z,\theta_i}$ is change of angle for rotating the antenna (vertical), Trans_{z,d_i} is the change in the position of link length position at

Table 2.1
D–H parameters for automation system.

Link	θ_i	α_i	a_i	d_i
	Degree		Millimeter	
1	$\pi/2$	$\pi/2$	0	X_{base}
2	$\pi/2$	$\pi/2$	0	Y_{base}
3	Θ_1	$\pi/2$	0	0
4	Θ_2	0	$l = 1$	0

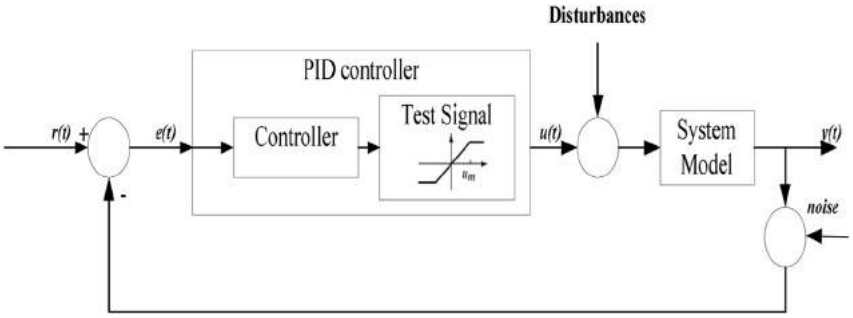

Fig. 3.1. Block diagram of control mechanism for prototype.

any arbitrary angle (vertical), Rot_{x,a_i} is change of angle for rotating the antenna (horizontal) and Trans_{x,a_i} is the change in position of the link length position change at any arbitrary angle (horizontal).

For any misalignment of antenna caused by minor mechanical tilting, arbitrary value of joint angle and link twist angle will eventually give the matrix as,

$$A = \begin{bmatrix} \cos\theta_i & -\sin\theta_i\cdot\cos\alpha_i & \sin\theta_i\cdot\sin\alpha_i & a_i\cdot\cos\theta_i \\ \sin\theta_i & \cos\theta_i\cdot\cos\alpha_i & -\cos\theta_i\cdot\sin\alpha_i & a_i\cdot\sin\theta_i \\ 0 & \sin\alpha_i & \cos\alpha_i & d_i \\ 0 & 0 & 0 & 1 \end{bmatrix} \quad (2.2)$$

Now, by inserting the D–H parameters presented in Table 2.1, we can arrive at the following 4 × 4 homogenous transformation matrices as

$$A_1 = \begin{bmatrix} 0 & 0 & 1 & 0 \\ 1 & 0 & 0 & 0 \\ 0 & 1 & 0 & X_b \\ 0 & 0 & 0 & 1 \end{bmatrix} \quad (2.3)$$

$$A_2 = \begin{bmatrix} 0 & 0 & 1 & 0 \\ 1 & 0 & 0 & 0 \\ 0 & 1 & 0 & Y_b \\ 0 & 0 & 0 & 1 \end{bmatrix} \quad (2.4)$$

$$A_3 = \begin{bmatrix} \cos\theta_1 & 0 & \sin\theta_1 & 0 \\ \sin\theta_1 & 0 & -\cos\theta_1 & 0 \\ 0 & 1 & 0 & 0 \\ 0 & 0 & 0 & 1 \end{bmatrix} \quad (2.5)$$

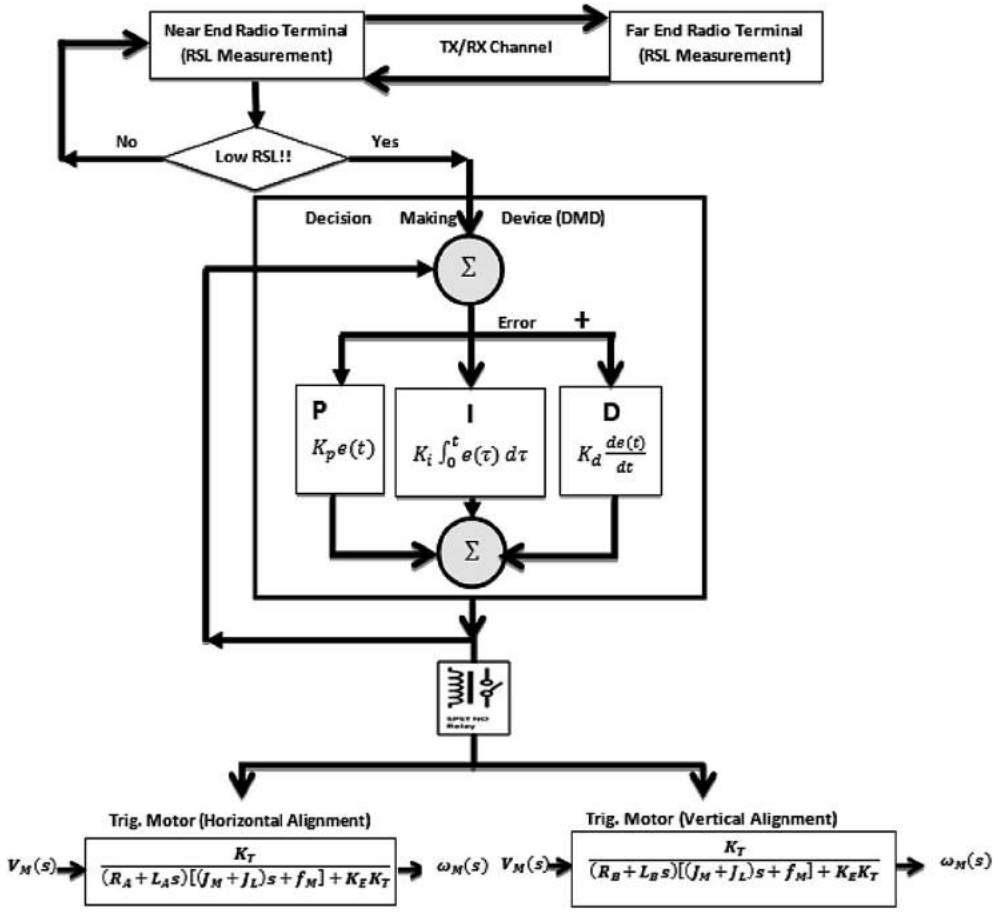

Fig. 3.2. Prototype analytical model for antenna realignment.

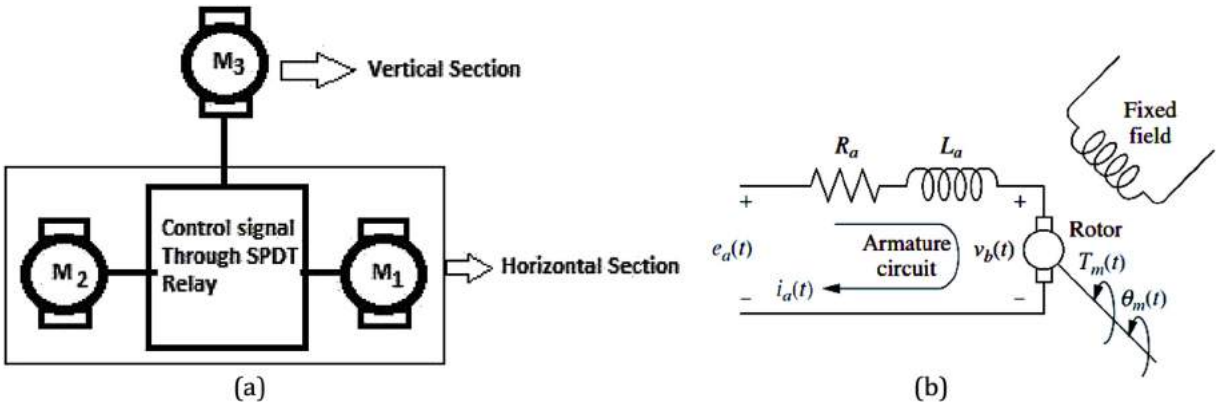

Fig. 3.3. (a) Block diagram representation of prototype motor utilization (b) Equivalent circuit of motor.

$$A_4 = \begin{bmatrix} \cos\theta_2 & -\sin\theta_2 & 0 & l\cdot\cos\theta_2 \\ \sin\theta_2 & \cos\theta_2 & 0 & l\cdot\sin\theta_2 \\ 0 & 0 & 1 & 0 \\ 0 & 0 & 0 & 1 \end{bmatrix} \tag{2.6}$$

Using product of A_1 & A_2 and A_3 & A_4 matrices, we arrive at the position and orientation of the toll frames indicated in Fig. 2.2(b) as

$$T = \begin{bmatrix} \sin\theta_1\cdot cos\theta_2 & -\sin\theta_1\cdot\sin\theta_2 & -\cos\theta_1 & \sin\theta_1\cdot\cos\theta_2 + Y_b \\ \sin\theta_2 & \cos\theta_2 & 0 & \sin\theta_2 \\ \cos\theta_1\cdot\cos\theta_2 & -\cos\theta_1\cdot\sin\theta_2 & \sin\theta_1 & \cos\theta_1\cdot\cos\theta_2 + X_b \\ 0 & 0 & 0 & 1 \end{bmatrix} \tag{2.7}$$

This T matrix signifies the required horizontal and vertical motion of the antenna. Equation (2.7), points to the position and orientation of loop antenna "R" in base coordinate system. Since the overall setup is adaptive in a sense that that alignment will be stopped after getting the desired RSL, henceforth θ_1 and θ_2 will constantly change with varied positions of X_{base} and Y_{base}. The work space is set using RCX controller through an inbuilt programming package.

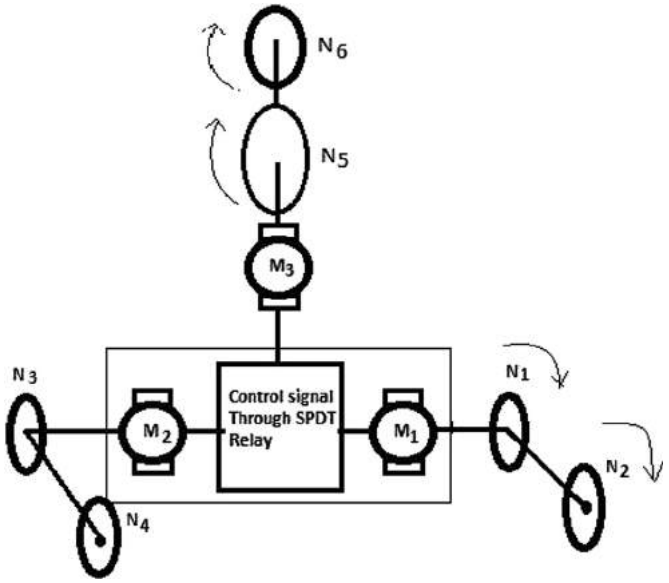

Fig. 3.4. Wheel rotation both for horizontal and vertical sections in prototype.

3. Model based simulation for prototype (tuning for optimal performance)

PID controller for the RCX Robonics kit administers the end-effector to reach a point $r(t)$, in this model; it is a pertinent RSL value which should be achieved by the antenna. It actuates the motor with a command $u(t)$ that rotates the end-effector horizontally or vertically thus measuring its position $y(t)$. It is done by means of a built in encoder which calculates the error $e(t) = r(t) - y(t)$ as a closed loop feedback system so that the $e(t)$ becomes zero and the system can achieve $r(t)$. A well-known general equation for this $u(t)$ can be presented as $u(t) = P(t) + I(t) + D(t)$. Based on aforementioned D–H model a block diagram of the control loop feedback mechanism is shown in Fig. 3.1. It describes the control architecture for two microwave antennas with (1 + 0) configuration placed to establish an MW link.

If the RSL of the transceiver drops below the desired threshold; a microcontroller will be triggered to mechanize the end-effector. Inside the RCX controller; there is PID tuning mechanism with proportional gain K_p, Integral gain K_i and derivative gain K_d. Based on the feedback pat; controller will always measure the RSL and activate the SPDT relay to operate two motors pertaining to horizontal and vertical movements of antenna. Model initially published in Ref. [10] was based on this principle and during observation, on an average; 2 out of 6 times both of the motors were rotating beyond their optimum positioning, thus only achieving the desired RSL with low response time. That is, the system was giving an overshoot response to achieve the required RSL. For this reason, tuning the controller with lower derivative gain would be possible solution to remove this overshoot. Fig. 3.2 represents an analytical model where antenna alignment is done based on PID controller.

In the last decade, development of automation for antenna alignment has been investigated by many researchers; some have come forward to give more accurate and efficient solutions. The core concept here is related with minimal time of solving alignment issue which intends to give high reliability of a system. Fig. 2.1 indicated in the prototype consists of two motors M_1 and M_1 which controls the horizontal movement while M_3 is responsible for vertical automation as we can see from block diagram representation in Fig. 3.3(a). Since we are focusing only on a pertinent movement at any given time; the relying mechanism is utilized. This brings forth an accumulative transfer function built on the basis of two movements of the end-effector.

In this model, a 9 V DC motor is utilized whose equivalent circuit is shown in Fig. 3.3(b). Based on this model, sectional transfer

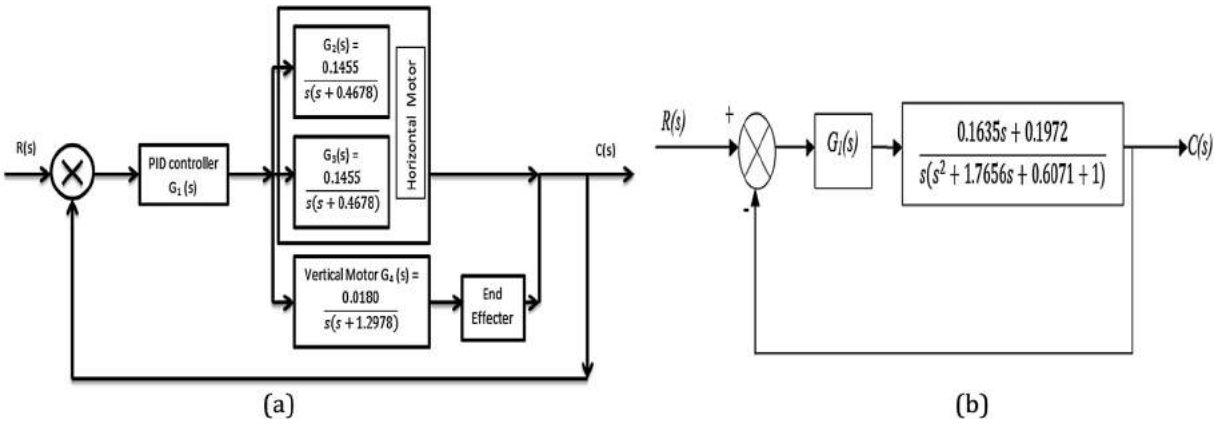

Fig. 3.5. Block diagram representation of prototype: (a) detail structure with transfer function; (b) reduced block.

function is analyzed. Both horizontal and vertical decks are equipped with two gears, approximately 8.5 in long conveyor belt joins the two gears, simultaneously; vertical section is loaded with prototype antenna (Fig. 2.1). Starting from a simple dc motor's transfer function, we join the mentioned mechanical parts to get the total transfer function. Using Fig. 3.3(b) and [19], horizontal DC motor M_1 has the transfer function as

$$\frac{\theta_{mr}}{E_{ar}} = \frac{\frac{K_{tr}}{(R_{ar}J_{mr})}}{s\left(s + \frac{1}{J_{mr}}\left(D_{mr} + \frac{K_{tr}K_{br}}{R_{ar}}\right)\right)} \tag{3.1}$$

where θ_{mr} = torque angle (subscript r is used to mention right), E_{ar} = applied armature voltage, K_{br} = back EMF constant, K_{tr} = motor torque constant, J_{mr} = equivalent armature inertia and load inertia reflected to the armature, R_{ar} = armature resistance and D_{mr} = equivalent damping (mechanical constant).

Now, inertia and damping constant is calculated by,

$$J_{mr} = J_{ar} + J_{Lr}\left(\frac{N_1}{N_2}\right)^2 \tag{3.2}$$

$$D_{mr} = D_{ar} + D_{Lr}\left(\frac{N_1}{N_2}\right)^2 \tag{3.3}$$

where, N_1 = number of rotation = 50, N_2 = number of rotation = 200, J_{ar} = armature inertia = 0.1 kg m^2, D_{ar} = armature damping = 0.01N ms/rad, J_{Lr} = load inertia = 0.5 kg m^2, D_{Lr} = load damping = 0.7 N ms/rad (All values are for a 7.2 V to 9 V DC servo motor as used in prototype.).

Using equations (3.2) and (3.3) we can get J_{mr} = 0.1374 kg m^2 and D_{mr} = 0.05375 N ms/rad. For this motor, torque vs. speed characteristics curve is useful to evaluate

a) Stall torque, $T_{stall} = (K_{tr}/R_{ar})e_{ar}$ = 0.19 N m,
b) No-load speed $\omega_{no\text{-}load} = (e_{ar}/K_{br})$ = 13.61 rad/s
c) Armature voltage e_{ar} = 7.2 V.

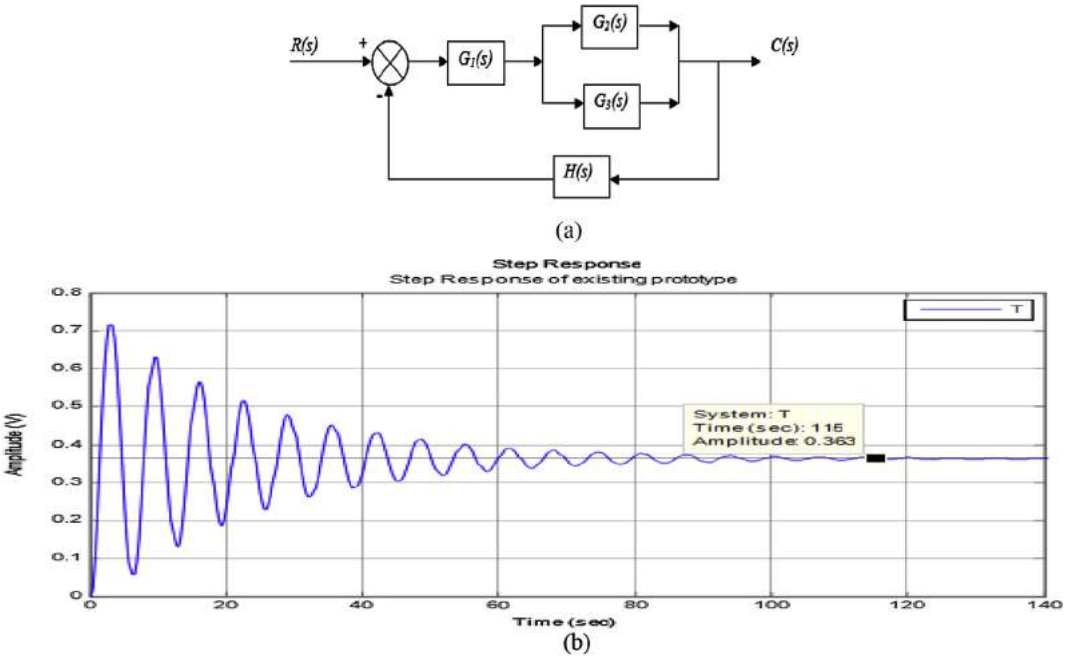

Fig. 4.1. Prototype representations – (a) in block diagram form; (b) step response.

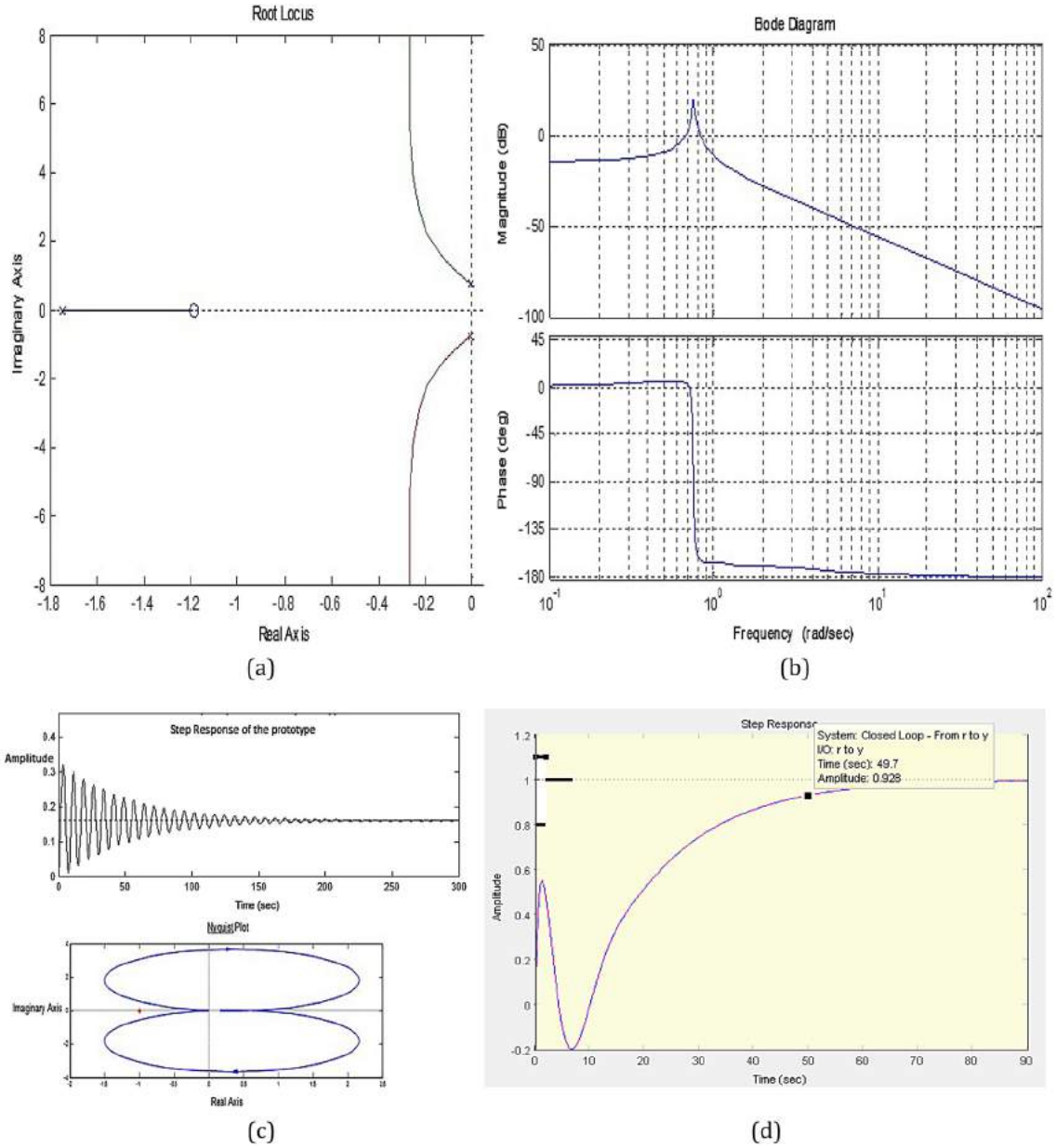

Fig. 4.2. System response – (a) root locus; (b) Bode plot; (c) step response, Nyquist plot; (d) open loop step response for model.

Here, electrical constants are $(K_{tr}/R_{ar}) = (T_{stall}/e_{ar}) = 0.02$ and $K_{br} = (e_{ar}/\omega_{no\text{-}load}) = 0.5290$. Now, by substituting all values in equation (3.1) we get,

$$\frac{\theta_{mr}}{E_{ar}} = \frac{0.1455}{s(s+0.4678)} \tag{3.4}$$

For motor M_2, number of turns N_3 and N_4 are similar to N_1 and N_2 aforementioned. Other parameter of M_2 is similar to M_1 thanks to the symmetry of utilizing bi-directional mobile base. For left side of horizontal section using the same procedure; transfer function of motor M_2 is evaluated as (subscript l indicates left side motor),

$$\frac{\theta_{ml}}{E_{al}} = \frac{0.1455}{s(s+0.4678)} \tag{3.5}$$

As in Fig. 3.4 vertical motor unit, two gears are utilized for coherence of rotation from motor to the end effecter. Gear labeled N_5 has rotation of 100 while N_6 will have 70 rotations. Armature inertia and damping constant is similar to that of M_1. Now, vertical motor inertia and damping constant is calculated by equations (3.6) and (3.7) (subscript v indicates vertical motor section),

$$J_{mv} = J_{av} + J_{Lv}\left(\frac{N_5}{N_6}\right)^2 \tag{3.6}$$

Table 4.1
System parameter of transfer function.

Observation	Eigen value	Damping factor (ζ)	Freq. (rad/s)
1	−7.68e − 003 +7.57e − 001i	1.01e − 002	7.57e − 001
2	−7.68e − 003 −7.57e − 001i	1.01e − 002	7.57e − 001
3	−1.74e + 000	1.00e + 000	1.74e + 000

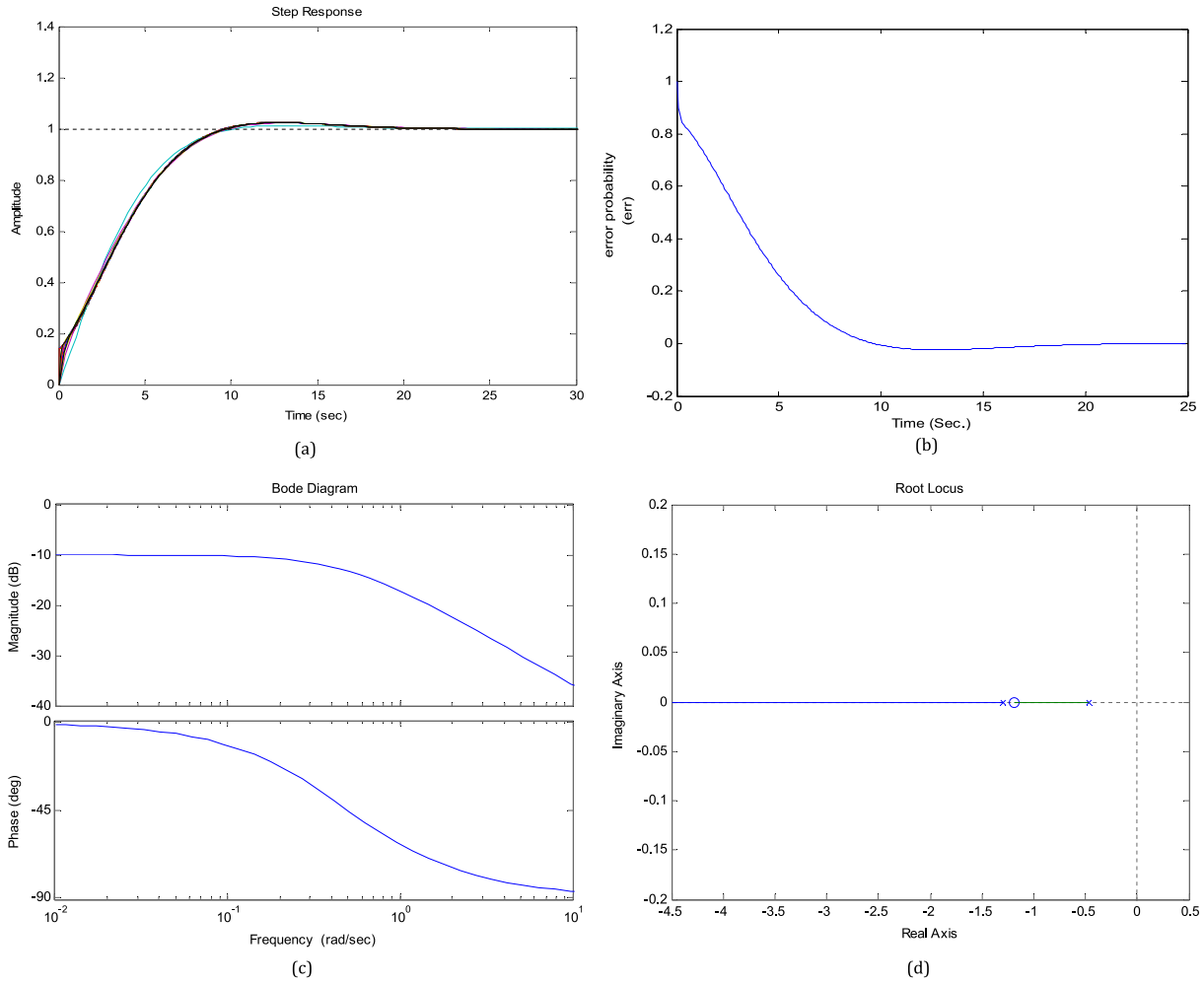

Fig. 4.3. System responses after tuning: (a) step response of prototype using filter; (b) error probability; (c) Bode plot; (d) root locus.

$$D_{mv} = D_{av} + D_{Lv}\left(\frac{N_5}{N_6}\right)^2 \tag{3.7}$$

which gives, $J_{mv} = 1.11$ Kg m^2 and $D_{mv} = 1.43$ N ms/rad and transfer function of vertical motor as,

$$\frac{\theta_{mv}}{E_{av}} = \frac{0.0180}{s(s + 1.2978)} \tag{3.8}$$

Equations (3.4), (3.5) and (3.8) can be represented as a block diagram system of the prototype shown in Fig. 3.5(a). Using block diagram reduction method the whole system is reduced to Fig. 3.5(b).

4. Model based analysis and system response of prototype

Based on the mechanism of Fig. 3.2, a generic block diagram of the control system is shown in Fig. 3.5(a) and (b). Detailed architectural analysis and further tuning for optimal performance is based on this model.

In Fig. 4.1(a), $R(s)$ is the input signal that is from initial RSL value, $C(s)$ is the output signal, $G_1(s)$ transfer function of basic PID controller built-in RCX, $G_2(s)$ and $G_3(s)$ are the transfer functions of horizontal and vertical motor unit respectively. $H(s)$ is the negative feedback path assuming with unity gain. Using the principle in Ref. [19], the complete transfer function of this system is,

$$F(s) = \frac{0.1635s + 0.1972}{s(s^2 + 1.7656s + 0.6071 + 1)} \tag{4.1}$$

Resultant block diagram of the system with aforementioned transfer function is shown in Fig. 3.5(b). Now, as discussed in PID controller tuning section about the existing prototype which has overshooting issue; by observing system step response, root locus and bode plot the exact values of overshoot can be deduced. Fig. 4.1(b) represents the prototype performance using a step input. As RCX controller is used, considering the simple case of K_p, K_d and K_i in the prototype, delayed value in terms of stability is observed with 115 s required to realign the antenna and restore the link which is undesired in case of BTS application.

Root locus plot in Fig. 4.2(a) shows the poles and zeros of the system and operational location. Dominant poles in the imaginary axis are responsible for the exponential variation i.e., the natural response. Real axis poles and zeros simply represent the forced response and it would be a criterion from general tuning system that by adding a pole, system would achieve stability more quickly. In present application of BTS system the prime focus is not only on the stability but also on system order that is why this idea is put aside for later work.

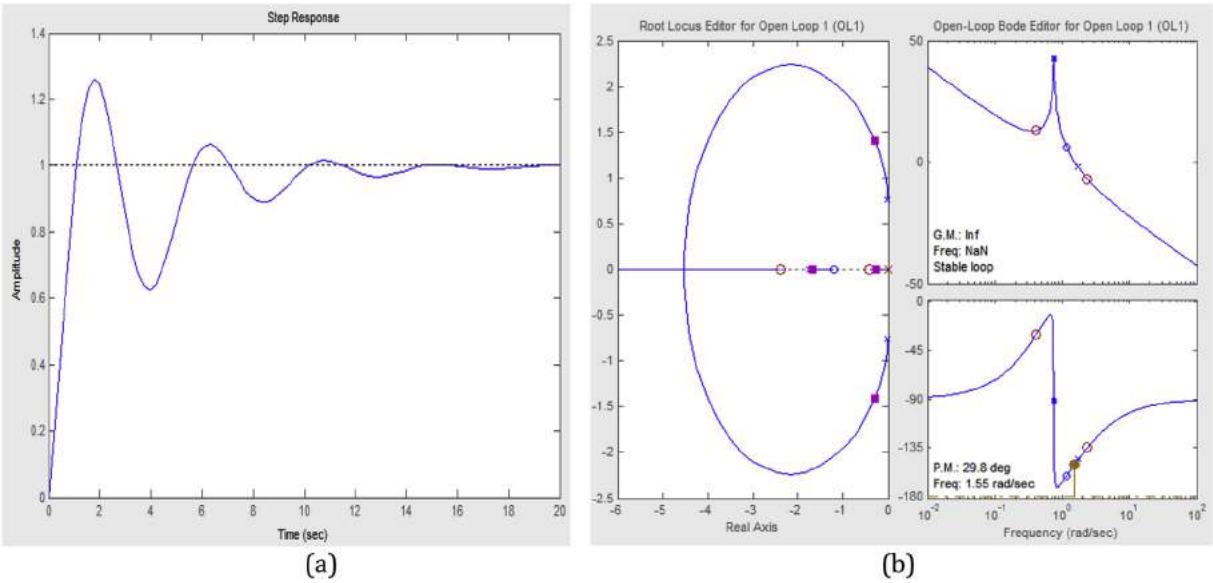

Fig. 4.4. System (a) step response; (b) root locus and bode plot after PID tuning.

Further to analyze the frequency response of developed prototype, Bode plot shown in Fig. 4.2(b) is presented. It can be safely said that any conventional second order system would have this type of response. Hence, the behavior near the break point is a strong function of the parameter ζ, which we call the damping factor. For small ζ the curve is peaked sharply near the corner frequency. Table 4.1 shows the simulated value of corresponding transfer function regarding damping factor and other related parameter in frequency domain. In observations 1 and 2, Eigen values are complex conjugate which depicts the system magnitude drops at −50dB/decade whereas 3rd observation shows a negative real Eigen value with higher damping factor but a steady magnitude response of approximate −10dB/decade.

4.1. Open loop system response

Graphical tool like SISO design in MATLAB is one of the interactive tools for system analysis and system response which is shown in Fig. 4.2(c) and (d). It shows the prototype step response and Nyquist plot. For step input system exhibit stable response after approximately 200 s which is nothing but the effect of derivative gain from RCX controller. In order to realign the antenna in time optimal manner, tuning technique should increase the response time and using rule of thumb; we can introduce an extra pole on real axis with dominant pole (Fig. 4.2(a)). Stability region of this model is shown by Nyquist plot in Fig. 4.2(c) where *x*-axis represents real part of our transfer function and *y*-axis is imaginary part. Open loop response of system represented in Fig. 4.2(d) gives a 10% overshoot and settling time of 2.0021 s. Observing this loop response; it is predictable that the initial response of this system needs further optimization.

4.2. Tuning method: PID tuning using low pass filter

As mentioned earlier about different tuning method of PID controller, amongst these, one with LPF is worked on. Although filter introduces some noise features, but minimizes the cost of solution. Moreover, based on the mathematical calculation we have decided to reduce our system parameter i.e. polynomial equation on denominator portion. Hence, step response after passing through LPF is shown in Fig. 4.3(a).

In Fig. 4.3(a), it can be observed that, a stable output is achieved within 22 s for the given closed loop system whereas previous system took between 115 and 150 s. Not only that, error probability of the system reaches minimum level within 25 s shown in Fig. 4.3(b). Compared to Fig. 4.2(b) representing previous model frequency response, the new tuned controller has been improved. In Fig. 4.3(c) there is no sign of damping factor based on simulation which can signify corner frequency and a smooth transition from lower frequency to higher frequency. Frequency response starts from −10dB/decade in magnitude for low frequency system decreases to −20dB/decade in high frequency. Root locus represented in Fig. 4.3(d) changes its orientation and now simply two poles and one zero lie on real axis. Operating region starts from dominant pole with angle of departure of 180° and ends in zero.

4.3. PID tuning with pre-filter and lead-lag compensator

In the second approach; the denominator polynomial is not minimized. Instead a PID tuning design method based on pre-filter and compensator along with the system and by using SISO tool for optimization; real time effect of the prototype can be extracted. System response with step input based on second approach gives a steady state response as depicted in Fig. 4.4(a) but prototype has to go through a certain amount of overshooting problem yet again.

Fig. 4.4(b) shows new root locus and bode plots using the tuning technique aforementioned. Compared to Fig. 4.2(c) and (d); it would be clear that changes in the locus point expresses a system which has at least 4 points of stability. Moreover, in negative real axis, additional pole has shifted 3 times from the dominant pole with respect to previous position. For this, step response is much better with minimal time for stability as 18 s. Corner frequency remains the same but effect of it is lower than previous frequency.

5. Conclusion

In this work, a new approach has been devised based on Denavit–Hartenberg parameters to autonomously realign an

MW link for any given communication system and particularly for terrestrial networks. As a result of this work, a prototype has been put forward that optimally realigns an MW antenna link based on reasonable time and best RSL value. Numerous control architectures have been rigorously designed and tested on combinatorial tools that include loop antenna as an end-effector with 2-DOF, RCX microcontroller, Comparator in LabVIEW to get desired RSL and time optimization to reach global minimum by means of controller design. Though this work is intended for BTS based antenna design, the underlying design can be used in applications where optimality is desired in terms of antenna directivity with time constraints. Though there is a potential of this study to solve alignment process, but it is described based on a prototype which have different parametric differences if we want to consider a practical scenario e.g., an average BTS height is about 70–90 m where MW antenna mounted on mechanical support, different cabling for power and networking. So, in order to implement such automated solution, motor selection, mechanical housing, weather proofing of the motor, and wind velocity to withstand the motor in critical situation is important for long run operation. These issues were not included on this study and can be taken as an extension to later work. Automation process has to be incorporated with BTS existing solution process. Because, RSL value will ensure alignment process is completed or not, henceforth it will be interesting to cast this work on actual environment.

Acknowledgment

The authors would like to acknowledge the supervision and guidance of Dr. Arild Moldsvor of Faculty of Electrical and Physics Engineering at Karlstad University, Sweden. Research facility for the project work was provided by Karlstad University, Sweden, Dept. of Electrical & Electronic Engineering, Int'l Islamic University Chittagong (IIUC), Bangladesh and Center of Intelligent Engineering Systems (CIES) at King Abdul Aziz University, Saudi Arabia.

References

[1] Exalt, Technical White Paper Microwave Fundamentals Series Antenna Alignment for Terrestrial Microwave Systems, April 2014.
[2] D. Esmael, K. Aleksey, The impacts of antenna Azimuth and tilt installation accuracy on UMTS network performance, Bechtel Telecommun. Techn. J. (January 2001).
[3] D. Okamoto, Cavity Beam Orbit Tilt Monitor, Tohoku University, 2009.
[4] AlgoSec and Kevin Beaver, The Dangers of Network Security Complexity, Complexity of Network Environments Causes System Outages and Security Incidents, October 2012.
[5] R. Heera Singh, B. Rami Reddy, B.C.S. Rao, Design and implementation of antenna control servosystem for satellite ground station, Int. J. Electr. Eng. Technol. (IJEET) (July 2013).
[6] Luca Catarinucci, Riccardo Colella, Luca Mainetti, Vincenzo Mighali, Luigi Patrono, Ilaria Sergi, Luciano Tarricone, Near field UHF RFID antenna system enabling the tracking of small laboratory animals, Int. J. Antennas Propag. 2013 (June 2013).
[7] Shreeji S. Sheth, Sima K. Gonsai, Antenna position control systems, review and new perception, J Inf. Knowl. Res. Electron. Commun. Eng. (October 2013).
[8] A. Goldsmith, Wireless Communications, Cambridge University Press, 2005.
[9] R. Christopher, U. Sennur, D. Roy, Wireless systems and interference Avoidance, IEEE Trans. Wirel. Commun. (July 2002).
[10] Ahmed Kamal Hassan, Ahsanul Hoque, Automated microwave antenna alignment of base transceiver station-time optimal link alignment, ATNAC (2011).
[11] P. Petrovic, R. Balogh, Wireless Radio Communication with RCX, 2006. IDI Technical Report 1.
[12] M.W. Spong, S. Hutchinson, M. Vidyasagar, Robot Dynamics and Control, second ed., Jan 2004.
[13] D. Sagris, S. Mitsi, K.D. Bouzakis, Gabriel Mansour, Spatial RRR robot manipulator optimum geometric design by means of a hybrid algorithm, Rom. Rev. Precis. Mech. Opt. Mechatron. (2011).
[14] M.D.S. Gomes, A.M. Ferreira, Manipulator control on a mobile robot, in: 2004-ABCM Symposium Series in Mechantronics, Feb 2012.
[15] W. Gawronski, Control and Pointing Challenges of Antennas and (Radio) Telescopes, November 15, 2004. IPN Progress Report 42-159.
[16] Nourin Kadir, Ariq I. Aziz, Sarjana J. Chowdhury, Samiha Shamma, Mohammed Tarique, Performance improvement of the tracking system of a satellite laser communication, Int. J. Comput. Appl. 26 (6) (July 2011) 19–25.
[17] Marcos César Rafael, João Bosco Gonçalves, Pedro Paulo Leite do Prado, Development of an automated system for maneuvering parabolic dish antennas used in satellite communication, in: ABCM Symposium Series in Mechatronics – Section II – Control Systems, vol. 5, p. 68–78.
[18] Mohammed Ahmed, Samsul Bahari B. Mohd Noor, Mohd Khair B. Hassan, Azura Bt Che Soh, A review of strategies for parabolic antenna control, Aust. J. Basic Appl. Sci. 8 (7) (May 2014) 135–148.
[19] Norman S. Nise, Control System Engineering, sixth ed., 2006. Chapter 2, p. 81, Chapter 5, p. 246.